Interaction of photosystem I from *Phaeodactylum tricornutum* with plastocyanins as compared with its native cytochrome c_6: reunion with a lost donor

[1]*Pilar Bernal-Bayard*, [2]*Chiara Pallara*, [1]*M. Carmen Castell*, [1]*Fernando P. Molina-Heredia*, [2]*Juan Fernández-Recio*, [1]*Manuel Hervás and* [1]*José A. Navarro**

[1]Instituto de Bioquímica Vegetal y Fotosíntesis, Universidad de Sevilla and CSIC, Américo Vespucio 49, 41092-Sevilla, Spain

[2]Joint BSC-CRG-IRB Research Program in Computational Biology, Life Sciences Department, Barcelona Supercomputing Center, Barcelona 08034, Spain

jnavarro@ibvf.csic.es

*Corresponding author: José A. Navarro. Instituto de Bioquímica Vegetal y Fotosíntesis, Centro de Investigaciones Científicas Isla de la Cartuja, Universidad de Sevilla & CSIC, Américo Vespucio 49, 41092-Sevilla, Spain. Tel.: 34-954-489-515; Fax: 34-954-460-165; E-mail: jnavarro@ibvf.csic.es

Abbreviations:

2

ß-DM, ß-dodecyl-maltoside; Cyt, cytochrome c_6; ET, electron transfer; k_2, second-order rate constant; k_2^{HI}, second-order rate constant at high ionic strength; K_A, equilibrium constant for the complex formation reaction; k_{ET}, first-order electron transfer rate constant; k_{ON} and k_{OFF}, association and dissociation rate constants, respectively, for complex formation; k_{OBS}, observed pseudo first-order rate constant; k_{SAT}, first-order limiting rate constant at infinite protein concentration; Pc, plastocyanin; PSI, photosystem I.

ABSTRACT

In the *Phaeodactylum tricornutum* alga, as in most diatoms, cytochrome c_6 is the only electron donor to photosystem I, and thus they lack plastocyanin as an alternative electron carrier. We have investigated, by using laser-flash absorption spectroscopy, the electron transfer to *Phaeodactylum* photosystem I from plastocyanins from cyanobacteria, green alga and plants, as compared with its own cytochrome c_6. Diatom photosystem I is able to effectively react with eukaryotic acidic plastocyanins, although with less efficiency than with *Phaeodactylum* cytochrome c_6. This efficiency, however, increases in some green alga plastocyanin mutants mimicking the electrostatics of the interaction site on the diatom cytochrome. In addition, the structure of the transient electron transfer complex between cytochrome c_6 and photosystem I from *Phaeodactylum* has been analyzed by computational docking and compared to that of green lineage and mixed systems. Taking together, the results explain why the *Phaeodactylum* system shows a lower efficiency than the green systems, both in the formation of the properly arranged [cytochrome c_6-photosystem I] complex and in the electron transfer itself.

1. INTRODUCTION

Diatoms are unicellular photosynthetic eukaryotes that are estimated to contribute to 30-40% of the global carbon fixation in the oceans, and thus can be considered major primary producers (1, 2). Diatoms have a complex evolutionary history, belonging to the red lineage of alga that diverged along evolution from the green lineage that led to plants (3, 4). Consequently, the photosynthetic machinery in diatoms possesses some singularities, arising from their evolutionary history and endosymbiotic origin (5-7). In particular, while most cyanobacteria and unicellular green algae contain both the copper-protein plastocyanin (Pc) and the iron-containing cytochrome c_6 (Cyt) as alternative soluble electron carriers between the b_6f and photosystem I (PSI) membrane complexes, most diatoms lack Pc, thus containing Cyt as the only soluble carrier between these complexes (8), with the remarkable exception of the oceanic centric diatom *Thalassiosira oceanica*, for which the presence of an unusual Pc has been reported (9).

In green alga and plants (the green lineage of photosynthetic eukaryotes), the very acidic donor proteins to PSI interact, by means of strong attractive electrostatic interactions, with a well-conserved positively-charged docking site located in an extra loop extension of the PsaF subunit in PSI (10-12). However, PSI from cyanobacteria, where both Pc and Cyt can be acidic, neutral or basic, lacks this extra loop, and thus the role of electrostatic forces in the interaction with PSI varies consequently (13-16). By its turn, although the evolution of the electron transfer (ET) to PSI in diatoms has also led to complementary electrostatic interactions between acidic and basic patches in Cyt and the PsaF subunit, respectively, the electrostatic character of both partners is similarly reduced, the intensity of the interaction being accordingly weakened as compared with the strongest electrostatic properties of the Cyt(Pc)/PSI complex in the green lineage (17).

4

Although the ET from Pc and Cyt to PSI usually follows similar mechanisms in the same organism, electron donation to PSI has increased in complexity and efficiency in eukaryotic cells as compared with prokaryotic cyanobacteria (13, 18-20). Recently, the ET reaction mechanism from Cyt to PSI from the diatom *Phaeodactylum tricornutum* has been first analyzed by laser-flash absorption spectroscopy (17), indicating that ET occurs within a Cyt/PSI transient complex that undergoes a reorganization process from the initial encounter complex to the optimized final configuration, as already described in "green" PSI systems. However, the results also demonstrated that the "red" *Phaeodactylum* system possesses a lower efficiency than "green" systems, both in the formation of the properly arranged [Cyt-PSI] complex and in the electron transfer itself (17). In addition, the relatively weak electrostatically attractive nature of the Cyt/PSI interaction seems to represent a compromise between the efficiency in the ET process and the need for a fast exchange of the protein donor (17).

In this work, the structure of the transient electron transfer complex between Cyt and PSI from the diatom *Phaeodactylum tricornutum* has been modeled by computational docking, and compared with that from green systems. Moreover, we have studied the cross-reactions between *Phaeodactylum* PSI and different prokaryotic and eukaryotic Pcs –including some mutant variants– in order to obtain relevant data on the differences and similarities of the diatom couple with respect to other well characterized systems, and on the evolution of the reaction mechanism in the different branches of photosynthetic organisms.

2. EXPERIMENTAL PROCEDURES

2.1. Protein purification

PSI particles from the diatom *Phaeodactylum tricornutum* were obtained by β-dodecyl-maltoside (ß-DM) solubilization as previously described (17). Pcs from the cyanobacterium *Nostoc* sp. PCC 7119, the green alga *Monoraphidium braunii* and the plant *Arabidopsis thaliana* were purified as described elsewhere (21, 22). Fern *Dryopteris crassirhizoma* Pc was generously provided by Prof. Marcellus Ubbink (Leiden University, The Netherlands). *Chlamydomonas reinhardtii* Pc and *Phaeodactylum* Cyt were obtained by cloning and expression in *Escherichia coli* cells using synthetic genes from the available database protein sequences, but with the codon usage optimized for *E. coli*, and fused in the amino-terminal to the transit peptide of Cyt from *Nostoc* sp. PCC 7119 (23). Protein purifications from the periplasmic fractions were carried out as previously described (17, 21). *Chlamydomonas* Pc mutants were generated by site-directed mutagenesis using oligonucleotide pairs containing the sequence change desired (Figure S1, in Supplementary section). Single mutants were generated by mutagenic PCR using the synthetic Pc WT gene as template. However, in order to generate the double E85K/Q88R mutant, the E85K simple mutant was used as template. Mutant proteins purification was carried out with the same procedure than for the WT Pc with minor changes. In all cases protein fractions were concentrated and finally frozen at -80 ℃ until use. The correct expression of all the proteins was checked by MALDI-TOF mass spectrometry, to estimate molecular weights and to compare with the theoretical expected ones. The concentration of the Cyt and Pcs was calculated using the published extinction coefficients at 553 nm (reduced form, Cyt) or 597 nm (oxidized form, Pcs) (21). The P700 content in PSI samples was calculated from the photoinduced absorbance changes

at 820 nm using the absorption coefficient of 6.5 mM^{-1} cm^{-1} determined by Mathis and Sétif (24). Chlorophyll concentration was determined according to Arnon (25).

2.2. *Laser flash absorption spectroscopy*

Kinetics of flash-induced absorbance changes associated to PSI reduction were followed at 830 nm as previously described (17, 26). Unless otherwise stated, the standard reaction mixture contained, in a final volume of 0.2 mL, 20 mM Tricine-KOH, pH 7.5, 10 mM MgCl$_2$, 0.03% ß-DM, an amount of PSI particles equivalent to 0.5 mg Chl mL^{-1}, 0.1 mM methyl viologen, 2 mM sodium ascorbate and Cyt or Pc at the indicated concentration. To study the ionic strength effect, the NaCl concentration was progressively increased by adding small amounts of a concentrated salt solution to the reaction cell. All the experiments were performed at 22 ºC in a 1 mm path-length cuvette. Kinetic data collection and analyses were as previously described (18, 26). Each kinetic trace was the average of 8-12 independent measurements. The estimated error in the observed rate constant (k_{OBS}) determination was ≤15%, based on reproducibility and signal-to-noise ratios. For the *Phaeodactylum* Cyt/PSI native system biphasic kinetic profiles were fitted according to a minimal three-step reaction mechanism involving intracomplex partners rearrangement (18, 27). Values for k_{ON} and k_{OFF}, the association and dissociation rate constants, respectively, for Cyt/PSI complex formation (and the equilibrium constant, $K_A = k_{ON}/k_{OFF}$), the ET first-order rate constant (k_{ET}), the first-order limiting rate constant at infinite protein concentration (k_{SAT}), and the amplitude of the fast phase for PSI reduction extrapolated to infinite Cyt concentration (R_{MAX}), were estimated as previously described (27) (Figure S2, in Supplementary section). For the Pc/PSI cross-reactions, monophasic kinetic profiles were fitted according to a more simple two-step reaction mechanism (18, 28). Minimal values for k_{ON}, and k_{OFF} (and K_A), as well as the

k_{SAT} values (equal to k_{ET}) were estimated applying the formalism previously described (28) (Figure S2, in Supplementary section) by a nonlinear least-squares computer-fitting iterative procedure using the KaleidaGraph program fitting routine.

2.3. Redox Titrations

The redox potential value for WT and each mutant *Chlamydomonas* Pc was determined as reported previously (15) by following the differential absorbance changes at 597 minus 500 nm. Errors in the experimental determinations were less than ±5 mV.

2.4. Structural modeling of proteins

The *Phaeodactylum* PSI complex was built as follows. PsaA and PsaB subunits were modeled based on the X-ray crystal structures of PsaA and PsaB from *Pisum sativum* (PDB 2WSC), with which they shared 79% and 76% sequence identity, respectively (29). The *Phaeodactylum* PsaF subunit was modeled based on the theoretical model of PsaF (30) from *Phaseolus aureus* (PDB 1YO9), with which it shared 51% sequence identity (slightly better than PsaF from spinach in PDB 2WSC, which had 48% sequence identity with *Phaeodactylum* PsaF). In addition, in this theoretical model the well conserved positively-charged PsaF residues (K16, R17, K23, K24), expected to be involved in the binding to the donor metalloproteins, are more exposed (especially K23) and seem to be in a better orientation than in the spinach PsaF X-ray crystal structure of PDB code 2WSC. All the sequence alignments were performed using BLAST (31). Then, a total of ten homology models were built using MODELLER version 9v10 with default settings (32), and the model with the best DOPE score (33) was finally selected.

Mutants of Pc from *Chlamydomonas* (E85K, Q88R, E85K/Q88R, E85V and V93K) were modeled with UCSF Chimera program (34), using the WT Pc crystal structure (PDB entry 2PLT) (35) as scaffold.

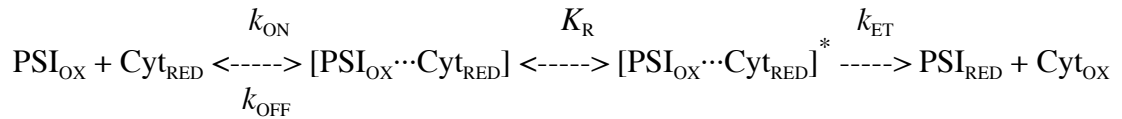## 2.5. Protein-protein docking simulations

Docking simulations were performed by FTDock (36) with electrostatics and 0.7 Å grid resolution and ZDOCK 2.1 (37), which generated 10,000 and 2,000 rigid-body docking poses, respectively. All docking poses were evaluated by the energy-based pyDock 1.0 scoring scheme (38), based on desolvation and electrostatics, with limited van der Waals energy contribution. Cofactors and ions were both included during the sampling and the scoring calculations, using a recently revamped version (upcoming publication) of pyDock 3.0 (39). After scoring, each docking pose was inserted in a bilayer lipid membrane using the Membrane Builder tool in the CHARMM-GUI website (http://www.charmm-gui.org) (40) with default parameters. Finally, all the docking solutions in which the soluble electron carrier was clashing with the membrane (i.e., any Pc or Cyt atom within a distance of less than 3 Å from any lipid molecule of the membrane) were removed. Atomic distances and clashes were computed with ICM-Browser program (41) (www.molsoft.com).

3. RESULTS

3.1. Kinetic analysis

In *Phaeodactylum*, Cyt acts as the only electron donor to PSI since this organism, as most diatoms, lacks Pc (3, 8). Here, by using laser-flash absorption spectroscopy, we have analyzed cross-reactions between Pc donor proteins from cyanobacteria, green alga and plant species with *Phaeodactylum* PSI. The rationale of this study is to check if diatom PSI still recognizes the lost Pc donor, and thus to shed new light on the evolution of the ET mechanism to PSI in the different branches of the evolutionary tree of photosynthetic oxygenic organisms.

Control experiments analyzing the interaction of cloned WT diatom Cyt with PSI showed biphasic kinetics for the re-reduction of photooxidized P_{700}^+ by Cyt (not shown), the Cyt concentration dependence of the k_{OBS} for both phases confirming the occurrence of the mechanism previously described for the *Phaeodactylum* Cyt/PSI couple and other eukaryotic donor/PSI systems (13, 17, 18, 27, 42-44):

$$PSI_{OX} + Cyt_{RED} \underset{k_{OFF}}{\overset{k_{ON}}{<----->}} [PSI_{OX}\cdots Cyt_{RED}] \overset{K_R}{<----->} [PSI_{OX}\cdots Cyt_{RED}]^* \overset{k_{ET}}{----->} PSI_{RED} + Cyt_{OX}$$

Where K_A corresponds to k_{ON}/k_{OFF}, K_R is the equilibrium constant for the rearrangement of the initial transient complex to achieve an optimized ($[PSI_{OX}\cdots Cyt_{RED}]^*$) ET configuration, and k_{ET} is the ET rate, which approximates to the k_{OBS} of the initial fast phase (ca. 20,000 s^{-1}; not shown), that in *Phaeodactylum* does not represent more than ≈30% of the kinetics amplitude (not shown) (17). The K_A value, estimated by using the formalisms previously reported (27) is shown in Table 1 together with k_{SAT}, the first-order limiting rate constant of the predominant slower phase at infinite protein

concentration (Figure 1, left) that not discriminates the rate for rearrangement from the pure intracomplex ET reaction. All the observed kinetics features are similar to those previously described for the Cyt purified from diatom cells (17).

When studying the interaction of Pcs with *Phaeodactylum* PSI, only monophasic kinetics were observed (Figure 2A), even though the protein concentration dependence of k_{OBS} exhibits in some cases saturation profiles (some examples are shown in Figure 1, left). It is important to mention that a possible fast kinetic component (if any) with a low amplitude (≤ 10 % of total absorbance change) would be not detectable in our system, due to the signal to noise ratio of the kinetic traces (Figure 2). Consequently the results have been here analyzed considering a more simple mechanism, consisting in transient complex formation without any detectable rearrangement within the complex previous to the ET step (13, 19, 28):

$$PSI_{OX} + Pc_{RED} \overset{K_A}{\longleftrightarrow} [PSI_{OX}\cdots Pc_{RED}] \overset{k_{ET}}{\longrightarrow} PSI_{RED} + Pc_{OX}$$
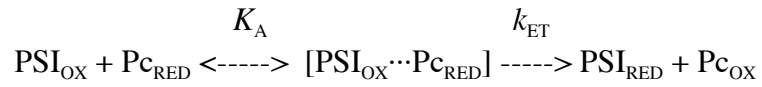
Where the estimated k_{SAT} limiting rate constant of the observed single kinetic phase at infinite Pc concentration now corresponds to the protein-independent k_{ET} rate (18, 28). Figure 1 also includes, for comparative purposes, the concentration dependence of the slower (and predominant) phase of the *Phaeodactylum* Cyt/PSI system. The estimated K_A values (equal to k_{ON}/k_{OFF}) for acidic Pcs are comparable to that calculated for the *Phaeodactylum* native system ($\approx 1 \times 10^4$ M^{-1}; Table 1). However, all these Pcs exhibited lower k_{SAT} (i.e., k_{ET}) values (ca. 300-400 s^{-1}) as compared both with the k_{SAT} of the slower phase (ca. 900 s^{-1}) (Table 1) and the k_{ET} (20,000 s^{-1}) of the diatom system, indicating the formation of less-optimized Pc/PSI ET complexes. On the other hand, in the case of Pcs from the cyanobacterium *Nostoc* and the fern *Dryopteris*, much slower kinetics (not shown) with k_{OBS} values depending linearly on Pc concentration were

obtained (Figure 1, left), indicating the occurrence of a simple oriented collisional mechanism, with no formation of transient complex (13, 19). Table 1 shows values for the second-order rate constants (k_2) inferred from such linear protein concentration dependence. Thus, whereas diatom PSI is able to effectively bind eukaryotic acidic Pcs, although with a minor ET efficiency as compared with *Phaeodactylum* Cyt (Figure 1 and Table 1), both the positively-charged *Nostoc* Pc and the fern Pc, in which the relocation of the acidic region results in very distinct electrostatic properties (45, 46), showed a drastic decrease in the affinity and the ET efficiency to PSI. Finally, the absence of a detectable fast phase when any Pc acts as electron donor to diatom PSI points to the subtle and precise interactions involved in the rearrangement process leading to the optimized configuration for ET in the native Cyt/PSI diatom couple (17).

Considering the different electrostatic features of *Phaeodactylum* Cyt and the different Pcs (8, 17, 20), an analysis of the effect of ionic strength on the process was also performed (Figure 1, right; and Figure 2B). As previously shown, the dependence of k_{OBS} for the predominant slower phase of PSI reduction in the native Cyt/PSI system on NaCl concentration showed a bell-shaped profile when increasing ionic strength, indicating the existence of some reorientation of redox partners inside the transient complex prior to the ET step [(17); and see below]. Regarding the Pc/PSI interaction, cyanobacterial and eukaryotic Pcs behave in an opposite way when increasing NaCl concentration (Figure 1, right). Thus, eukaryotic Pcs interact with diatom PSI by means of attractive forces, as inferred from the continuous decrease of the k_{OBS} at increasing salt concentrations. However, *Nostoc* Pc shows repulsive electrostatic interactions with the diatom PSI, as deduced from the increase of the k_{OBS} when increasing NaCl. Table 1 shows the second-order rate constants values (k_2^{HI}) estimated at high ionic strength (200 mM NaCl concentration) for the different donor/PSI systems. It is interesting to note that, with the

exception of the divergent fern Pc, the k_2^{HI} values at high ionic strength are similar, but also sensibly lower than that obtained with the diatom Cyt, indicating that the intrinsic reactivity of the different Pcs with PSI in the absence of electrostatic interactions is similar, but lower than the native Cyt. This behaviour could be explained by the different intrinsic efficiency of cofactors –exposed heme vs. a hindered Cu cofactor– or different surface steric properties.

From the solved crystal structure of *Phaeodactylum* Cyt, turns out that this protein has evolved towards a decrease in the acidic area thought to be involved in the interaction with PSI [revised in (47), and see (8, 17)] (Figure 3). Taking into account the different intensity in the electrostatic character of *green* Pcs and the diatom Cyt, a set of *Chlamydomonas* Pc mutants were constructed by replacing negative residues by neutral or positive groups (Figure 3) in order to mimic the Cyt properties, and so trying to increase in this way the Pc ET efficiency with PSI. Although *Arabidopsis* Pc showed to be slightly more reactive than *Chlamydomonas* Pc, the green alga protein was selected because its closer evolutive relation with the diatom. When analyzing the reduction of *Phaeodactylum* PSI by the mutated Pcs, no fast phase was observed in most cases, although the non-linear donor protein concentration dependence of k_{OBS} shown in Figure 4 (left) again indicates the formation of transient bimolecular complexes. The estimated minimal values for K_A and k_{ET} for the different Pc mutants are shown in Table 1. The only exception to this behavior is the Q88R mutant, for which biphasics kinetics were observed at Pc concentration ≥ 150 μM (not shown). However, the very low amplitude of the initial fast phase (<15%) does not allow to obtain reliable k_{OBS} values ($\approx 1,000$ s^{-1}, not shown), which are in any case of the same order of magnitude as the saturation value of the slower phase at high protein concentration (ca. 600 s^{-1}, Table 1). Thus the occurrence of the kinetic mechanism involving complex formation without intracomplex protein

rearrangement was here assumed for the interaction of this mutant with PSI. In addition, this mutation brings back one arginine residue into the northern surface of *Chlamydomonas* Pc that has been previously described as important for the binding to PSI in prokaryotic Pcs (15).

The kinetic data shown in Table 1 indicate a moderate effect of the different Pc mutations at low ionic strength. Thus, the E85K and Q88R Pc showed a slightly increased efficiency in the ET to PSI, whereas mutants E85V, V93K and E85K/Q88R, displayed a diminished reactivity towards PSI. In the case of the E85K and Q88R mutants, the less saturated profiles at high donor concentration, as compared both with the WT Pc and the other mutants (Figure 4), generates a higher inaccuracy in the determination of the kinetic constants (Table 1). However, this behaviour already reflects a diminished K_A towards PSI, as also indicated by the lower estimated values. It is interesting to note that these two mutants showing the lower K_A values (E85K and Q88R) also have the higher k_{ET} rates. The opposite effect is observed in the E85V Pc, in which a higher affinity in the binding to PSI is accompanied by the lower efficiency in the ET reaction (Table 1). The different effect of the mutations has to be explained mostly in terms of changes in the electrostatics of protein surfaces or steric modifications induced by the aminoacid replacements, as the redox potential is not significantly altered in the Pc mutants (Table 1), with the only exception of the E85K/Q88R double mutant, for which a ca. 20 mV potential increase would only partially explain the diminished k_{ET}. In addition, the effect of the mutations can be highlighted when analyzing the effect of increasing ionic strength on PSI reduction by the different Pc mutants (Figure 2C; and Figure 4, right). As indicated before, WT Pc showed a marked decrease of the k_{OBS} with increasing salt concentration, thus reflecting relatively strong attractive interactions with PSI. However, all the mutants present a dependence on ionic strength much smoother than the

WT protein, which is again particularly relevant in the case of the E85K and Q88R Pcs, both mutants being significantly more reactive towards PSI than the WT Pc as the salt concentration increases (Figure 2B and 2C; and Figure 4, right), and consequently showing in both cases higher k_2^{HI} values (Table 1).

3.2. Structural model of Cyt/PSI interaction by computational docking

To understand the structural and energetic determinants of the differences in efficiency observed in diatom PSI reduction with respect to the green systems (17), computational docking simulations were performed between the modeled structure of PSI from *Phaeodactylum* (see Methods) and both its native Cyt (PDB entry 3DMI) (8) and the corresponding Cyt from the green alga *Monoraphidium* (PDB entry 1CTJ) (48), for which kinetic data for the ET to diatom PSI have been previously reported (17). We note that while we were preparing this manuscript, a new structure for PSI from *Pisum sativum* (PDB 4Y28) has been reported (49), with a slightly better sequence identity with *Phaeodactylum* PsaF (53%). Actually, the theoretical model that we used as template for PsaF has 1.6 Å Cα-RMSD from this new structure (4Y28), therefore much closer to it than the spinach PsaF structure (2WSC) that we used as template for PsaA and PsaB (2.8 Å Cα-RMSD). Even though the choice of one or another structure among the similar templates that are available for PsaF is not going to significantly affect the modeling, all the above considerations suggest that the choice of the theoretical model as template for PsaF was an appropriate decision.

The docking simulations between PSI and Cyt from *Phaeodactylum* showed a funnel-like binding energy landscape (Figure S3, in Supplementary section), with the lowest-energy docking orientations in which the residues W652 of PsaA and W624 of PsaB (which form the expected hydrophobic recognition site and the ET pathway to P700

for Cyt and Pc [50, 51]) and the propionate groups of the heme molecule of Cyt were located at a distance of around 10-20 Å (minimum distance among the top 20 docking poses is 8.1 Å) (Figure S3, in Supplementary section and Table 2). There are also docking orientations with short-distance between W652 of PsaA, W624 of PsaB and the Cyt heme, but at higher docking energy. This is consistent with the reorganization process from the initial encounter complex observed for this interaction [(17), and see above].

Remarkably, the docking between *Phaeodactylum* PSI and *Monoraphidium* Cyt yielded a much larger population of low-energy docking orientations in which PsaA W652, PsaB W624 and the Cyt heme were at very short distance (minimum distance among the top 20 docking poses is 2.8 Å) as compared with the native *Phaeodactylum* complex (Figure S3, in Supplementary section). This is consistent with the more efficient ET kinetics (and higher k_{ET}) to diatom PSI found when analyzing *Monoraphidium* Cyt as compared with the native protein, and with the smaller reorganization effect seen for this interaction (17). In addition, the docking poses for *Monoraphidium* Cyt showed better scoring values (average scoring for the top 20 docking poses is -39.9 a.u.) than for *Phaeodactylum* Cyt (average scoring for the top 20 docking poses is -32.7 a.u.) (Table 2). Since the docking scoring values can be related to the binding affinity, these findings are also consistent with the better association constant (K_A) found in the cross-reaction with *Monoraphidium* Cyt **(17)**.

We have analyzed in detail the most efficient docking models for ET (e.g., PsaA W652, PsaB W624 and Cyt heme groups at less than 3.0 Å distance) in the interaction of the diatom PSI with *Phaeodactylum* and *Monoraphidium* Cyt (Figure 5). The best energy model from *Phaeodactylum* Cyt docking (PsaA W652, PsaB W624 and Cyt heme at 3.0 Å distance) does not show electrostatics interactions with the conserved positive patch in

PsaF (Figure 5B), neither favourable interactions at the binding interface (Figure 5C). This can explain why the efficient docking orientations in the *Phaeodactylum* Cyt docking are energetically penalized. On the contrary, the best model from *Monoraphidium* Cyt docking shows strong electrostatic interactions between the conserved positive patch in PsaF and the Cyt residues D69, E70, D71, and E72 (Figure 5D and 5E) in the Cyt acidic patch, previously proposed to be involved in the interaction with PSI in green systems (12, 43, 51). Although this acidic patch is conserved in *Phaeodactylum* Cyt (residues S113, D114, E115 and E116) (8), as stated above these residues in *Phaeodactylum* Cyt are not interacting with PsaF in the ET efficient docking orientations. The reason for these differences in binding is that in *Monoraphidium* Cyt this docking orientation is further stabilized by electrostatic interactions between PsaA residues R747 and R648, and *Monoraphidium* Cyt residues D42 and H30 (Figure 5E). However, in *Phaeodactylum* Cyt these residues are A86 and K74, respectively, which thus can explain why an equivalent docking orientation would be energetically penalized in the interaction with *Phaeodactylum* PSI, and, as a consequence, other less-efficient orientations for ET become more populated (Figure S3A, in Supplementary section).

3.3. Structural model of Pc/PSI interaction by computational docking

We also applied computational docking to investigate the interaction between *Phaeodactylum* PSI and Pc from *Chlamydomonas*, both for the WT protein and mutant variants previously designed to try to mimic *Phaeodactylum* Cyt electrostatic properties (Pc mutants E85K, Q88R, E85K/Q88R, E85V and V93K) (Figure 3). In the WT Pc docking simulation, the 20 lowest-energy docking orientations had the PsaA W652, PsaB W624 residues and the Pc His87 residue [involved in the active-site catalytic triad (35, 43, 50)] at a distance above 4.2 Å (Figure S4, in Supplementary section). The average

docking scoring for these top 20 docking poses is -37.4 a.u. (Table 2). There are other docking poses with shorter distances between the redox groups (and therefore, expectedly more efficient for ET) but with clearly worse docking energies. In any case, the fact that the lowest-energy docking orientations have redox groups not very far from each other is consistent with the absence of reorganization effects for these interactions. According to the docking model, the minor ET efficiency of *Chamydomonas* Pc to *Phaeodactylum* PSI —as compared with the diatom Cyt— is not justified by a longer distance between redox groups in docking, but it should be again explained by an intrinsic different efficiency of cofactors and/or surface composition, given that they are essentially two different systems. A deep theoretical analysis of all these considerations would involve large quantum and molecular mechanics calculations, which are beyond the focus of the present work. On the other hand, when performing docking with Pc E85K and Q88R mutants, the 20 lowest-energy docking poses included models that had PsaA W652, PsaB W624 and Pc His87 located at very short distance (1.4 Å), with an average docking scoring of around -30 a.u. (Figure S4, in Supplementary section; and Table 2). This is consistent with the above described observation that these mutants slightly increased ET but decreased binding affinity.

It is interesting to analyze in atomic detail the results from the Pc/PSI docking. Figure 6 shows two representative models from the docking between *Phaeodactylum* PSI and *Chamydomonas* WT Pc. One (Figure 6B,C) is the best-energy model among the most efficient docking orientations for ET (e.g., PsaA W652, PsaB W624 and Pc His87 at less than 2.0 Å distance). More specifically, this docking model has PsaA W652, PsaB W624 and Pc His87 at a distance of 1.9 Å, and shows a strong electrostatic interaction between the conserved positive patch in PSI subunit PsaF and the Pc residues D42, E43 and D44 in the "east" negative patch (35), thus delineating an orientation equivalent to that above

described for *Monoraphidium* Cyt (compare Figures 5D and 6B). Interestingly, PsaA R747 is interacting with Pc residue N64 (located in same position as *Monoraphidium* Cyt D42 in the ET efficient docking model), and PsaA W652 is interacting with Pc H87 (Figure 6C). This shows that green Pc is able to form similar contacts as green Cyt with *Phaeodactylum* PSI for efficient ET. This docking orientation would not be affected in the E85K and Q88R mutants, and thus the reason of the effect of these mutations must be found in other docking orientations that are not so efficient for ET (see below).

In this sense, Figure 6 also shows the expectedly most efficient orientation for ET among the 20 lowest-energy docking models in which PsaA W652, PsaB W624 and Pc His87 are located at 4.2 Å distance (Figure 6D,E), which in principle would be less efficient for ET than the previously described docking model. In this new model, while there is still some electrostatic interactions with the conserved positive patch of PsaF subunit in PSI (Figure 6D), there are other interactions that could additionally contribute to its binding affinity, such as the one between Pc Q88 and PsaA K638, or more especially, between Pc E85 and PsaA R463 and R648 (Figure 6E). Replacement of these two Pc residues by positively charged ones, as in E85K and Q88R mutations, will cause destabilization of this docking orientation, which has redox centers at medium distance (and therefore not optimal for ET), and now the docking orientations with short distance between redox groups (expectedly more efficient for ET) would become more populated.

On the other side, in the docking simulations with the Pc mutants E85K/Q88R, E85V and V93K, no significant differences were found in the distribution of the low-energy docking pose orientations with respect to the WT (not shown). Indeed, the average docking energies for the top 20 docking poses were of -33.0, -35.2 and -37.3 a.u., for which the minimum distance between PsaA W652, PsaB W624 residues and Pc H87 were 3.2, 4.2 and 4.1 Å respectively (Table 2).

4. DISCUSSION

PSI reduction has been extensively analyzed *in vitro* and *in vivo* in a wide variety of organisms, revealing that the kinetic mechanisms for the reaction of either Pc or Cyt with PSI from the same organism are similar, although they have increased in complexity and efficiency while evolving from prokaryotic cyanobacteria to green alga and plant eukaryotic organisms (13). Thus, PSI reduction by the donor proteins, isolated from different sources, can follow either an oriented collisional mechanism (type I), a mechanism involving transient complex formation (type II), or complex formation with rearrangement of the interface (type III), the latter mechanism classically observed in green alga and plant eukaryotic systems (13).

It has been previously described that the ET reaction from Cyt to PSI in the diatom *Phaeodactylum* follows the type III three-steps mechanism found in eukaryotic green systems (17), in which an initial Cyt/PSI encounter complex reorganizes to a more productive final configuration. This is consistent with the docking models shown here, in which the most stable docking orientations are not expected to be efficient for ET due to the longer distance between redox centers. In addition, the diatom system shows lower efficiencies than the green systems both in the formation of the properly arranged [Cyt-PSI] complex and in the ET reaction itself (13, 17, 22, 27, 43, 50). This apparent decreased reactivity is the consequence of diminished basic patches on PsaF and acidic regions on Cyt, both resulting in a weaker electrostatic interaction between partners. This feature of diatoms has been proposed to denote a compromise between ET efficiency and optimal protein donor turnover (17), as in the green systems it has been suggested that the strong donor/PSI electrostatic interaction limits the donor exchange and so the overall ET turnover (12, 44).

It is interesting to compare the *Phaeodactylum* native Cyt/PSI docking complex (Figure 5B,C) with those described previously in green systems (10, 12, 43, 51). It is widely accepted that the lumenal loops i/j of PsaA/B in PSI, including the PsaA W651 and PsaB W627 residues (*Chlamydomonas* numbering), form the hydrophobic recognition site for binding of Pc and Cyt, by means of complementary hydrophobic areas around the donors ET site (43, 50). Electrostatic interactions are also established between negatively charged residues of Pc and Cyt with the positively charged N-terminal domain of PsaF (12, 51). Particularly, *Chlamydomonas* Cyt seems to establish specific interactions involving residues K23/K27 of PsaF and the E69/E70 groups located at the "eastern" negatively charged area of Cyt. Additionally, the positive charge on the "northern" site of Cyt (R66) and the adjacent D65 can form a strong salt bridge with the R623/D624 pair of PsaB (51). According to this model, the distance between the donor/acceptor redox cofactors is ≈14 Å (12, 51). The *Phaeodactylum* Cyt/PSI docking complex described here (Figure 5B,C) has a different orientation than the *Chlamydomonas* Cyt/PSI complex. The reason is that the D65 group in *Chlamydomonas* Cyt is not conserved in *Phaeodactylum* Cyt (equivalent residue is Gly109), and thus it cannot stabilize this orientation. As a consequence, it also loses the electrostatic interactions with PsaB and the overall binding energy is less favorable.

Cyt is the only electron carrier between the b_6f and PSI complexes in *Phaeodactylum*, and thus a pertinent question is if diatom PSI is still able to recognize the lost Pc donor. It is first interesting to note that *Nostoc* cyanobacterial Pc reacts with low efficiency with diatom PSI by means of a simple oriented collisional mechanism. This is in agreement with the low reactivity previously described in cross-reactions of Cyt/PSI systems from cyanobacteria and *Phaeodactylum* (17). On the other hand, most cross-reactions involving acidic green Pcs and diatom PSI show kinetic parameters comparable in the main limiting steps (intermolecular affinity and efficiency at saturating donor

concentration) to the native diatom system (Table 1), even though they follow different kinetic mechanisms. Thus, the interaction of green alga and plant Pcs with diatom PSI proceeds via transient complex formation, but apparently with the absence of the final rearrangement step observed in the native *Phaeodactylum* system, and with sensibly lower k_{ET} rates, indicating the formation of less-optimal functional complexes. This emphasizes the fine adjustment involved in the formation of the final productive structure in the Cyt/PSI diatom couple, that is lost in the interactions with the non-native Pc donors (17).

The results obtained in the cross-reactions should be explained according to the different structural and electrostatic features of Pcs from different sources, as well as of the donor docking site in diatom PSI. Thus, whereas the low efficiency in the interaction of the positively-charged *Nostoc* Pc agrees with the occurrence of repulsive electrostatic interactions with the also positively-charged binding site on the diatom PSI (17), eukaryotic acidic Pcs seems to interact with diatom PSI by means of attractive forces, as previously described for the interaction of *Monoraphidium* Cyt with *Phaeodactylum* PSI (17). However, it is interesting to note that, in spite of the different electrostatic character of Pcs from the different sources, the reactivity towards PSI at high ionic strength is very similar in most cases, indicating a comparable intrinsic reactivity of the different Pcs in the absence of electrostatic forces. This intrinsic reactivity is, nevertheless, about 4-5 times lower when compared with the diatom native system (Figure 1, and Table 1), suggesting that other factors beyond the pure electrostatics, i.e., hydrophobic and/or solvent effects or structural steric factors, contribute to this difference in reactivity.

Fern Pc represents an interesting exception to the main features of the reactivity of green Pcs with diatom PSI, as *Dryopteris* Pc shows the lowest efficiency of the systems here analyzed (up to ten times less efficient than the cyanobacterial *Nostoc* Pc). It has

been previously reported that fern Pc conserves both the same global structure and negative electrostatic character of eukaryotic Pcs, but its acidic region has moved from the canonical east position and is surrounding the hydrophobic ET north site, this change resulting in very distinct electrostatic and steric properties (45, 46). Thus, the unusual structure of *Dryopteris* Pc impedes an efficient interaction with diatom PSI, as previously described in its interaction with spinach PSI (46), confirming that fern Pc has followed a relatively independent evolutionary pathway since ferns diverged from other vascular plants (45, 46).

Previous results obtained with cross-reactions of different Cyt/PSI eukaryotic systems suggested that are mainly the different electrostatic properties of Cyt, more than the PSI, which make the difference in behavior of diatoms with respect to other photosynthetic eukaryotes from the green lineage (17). This has been confirmed here by computational modeling. The *Monoraphidium* Cyt/*Phaeodactylum* PSI docking complex shows virtually the same orientation as the native *Chlamydomonas* Cyt/PSI green complex, and is able to form similar interactions with the positive patch in PsaF (Figure 5D) (51). In addition, the salt-bridges formed by D65 and R66 of *Chlamydomonas* Cyt with PsaB R623 and D624 residues are conserved in the *Monoraphidium* Cyt/diatom PSI interaction (equivalent residues: D65 and R67; and R620 and D621, respectively). The key interface D42/R747 salt-bridge found in our *Monoraphidium* Cyt/*Phaeodactylum* PsaA model was not previously reported for the *Chlamydomonas* Cyt/PSI complex (51), but since these residues are conserved (equivalent ones are D41 and R746), we can expect that this salt-bridge is also formed in *Chlamydomonas* Cyt/PSI complex. Interestingly, the redox centers in *Monoraphidium* Cyt/*Phaeodactylum* PSI are found at a shorter distance (11.6 Å) than in *Chlamydomonas* Cyt/PSI ($\approx$ 14 Å) (51). In addition, the reduction of diatom PSI by the strongly acidic Cyt from green alga showed an increased

affinity and k_{ET} but a lower efficiency in the formation of the properly arranged Cyt/PSI complex as compared with the native Cyt, because the too strong electrostatic interactions (17). Thus, *Chlamydomonas* Pc mutants are here designed by replacing negative groups of the acidic patch –widely accepted to be responsible for electrostatic interactions with PSI (12, 35, 47)– by neutral or positive residues (Figure 3). The rationale for these designs has been to mimic the Cyt electrostatic properties, trying to increase the efficiency of a green Pc in reducing diatom PSI by decreasing the negative character of its acidic patch (Figure 3).

The effect of the different Pc mutations, although moderate, gives interesting information about the binding mechanism to PSI. Thus, higher k_{ET} rates, as compared with the WT Pc, are observed with the two mutants (E85K and Q88R) showing about half of the K_A value of the WT protein (Table 1). Just the opposite effect is however obtained in the E85V Pc, in which the lower k_{ET} rate goes together with the higher affinity towards PSI (Table 1). Actually, an inverse exponential relationship between the estimated K_A and k_{ET} values is observed for all the *Chlamydomonas* Pc variants (Table 1). Thus, WT *Chlamydomonas* Pc seems to be fixed, by means of strong electrostatic interactions, in a less productive complex configuration, that can be improved in mutants showing an increased flexibility in the binding to PSI. Our docking model shows that E85K and Q88R mutants are destabilizing this less productive complex configuration, which effectively increases the population of the productive orientations and therefore are more efficient for ET. In this sense it is interesting again to compare the docking model of *Chlamydomonas* Pc/diatom PSI with the previously proposed Pc/PSI interactions in green systems, in which electrostatic interactions involve D42/D44 and E43/E45 of Pc with residues K17/K23/K30 in PsaF (11, 12). The *Chlamydomonas* Pc/*Phaeodactylum* PSI most productive docking model (Figure 6B) conserves such interactions and thus

would be able to yield efficient orientations for ET. However, Pc E85 and Q88 residues are stabilizing alternative, but less productive, orientations in the *Chlamydomonas* Pc/diatom PSI complex (Figure 6E). This is consistent with the smaller ET efficiency found for *Chlamydomonas* Pc, and the ET increase in E85K and Q88R mutants. Interestingly, *Chlamydomonas* Pc does not possess a positively charged amino acid at a position equivalent to the R66 found in *Chlamydomonas* and *Phaeodactylum* Cyts (corresponding to the R87 position of prokaryotic Pcs). In cyanobacteria, this positively charged amino acid is important for efficient ET to PSI (15). Thus, by bringing back this arginine residue in the Q88R mutant of the green alga Pc, an improved reactivity has been observed.

On the other side, we should note that the effect of the two individual E85K and Q88R mutations is counteracted in the double mutant E85K/Q88R, which shows a similar K_A and a slightly diminished k_{ET} compared with the WT Pc. This would be at least partially explained in terms of the small increase of the double mutant redox potential. However, there must be some additional effect that cannot be described in our rigid-body docking simulations, like a conformational change of the two new positive residues that avoids the destabilization effect of the lesser productive configuration by the two individual mutations. Lastly, the results obtained with the V93K protein indicates that this hydrophobic residue is relevant in the ET process, as this mutant shows a significantly decreased k_{ET}, in spite of maintaining the same affinity for PSI than the WT Pc (Table 1).

To conclude, the kinetic and mutagenic analysis herein reported for *Phaeodactylum* PSI reduction by green Pcs contrasts with the results previously obtained with a eukaryotic Cyt (17). Whereas the green alga Cyt overall reacts more efficiently with diatom PSI than the native Cyt —both in affinity and ET rate— because its stronger

electrostatic character (17), green Pcs are together less efficient in the ET proccess, while maintaining a similar affinity than the *Phaeodactylum* Cyt towards diatom PSI. In addition, our analysis with mutated green alga Pcs shows that introducing positive groups, and thus weakening the interaction with PSI, can in some cases enhance the ET step. This is the result of an improved intracomplex flexibility to optimize ET, indicating that in the WT Pc too strong electrostatic interactions determine a non-optimal complex configuration of the redox partners. These differences in the Cyt/Pc interaction with the diatom PSI cannot be explained only in terms of dissimilarities in the electrostatics of the studied systems, but also in the existence of differential structural and steric factors in the two families of soluble electron carriers.

Conflict of interest

The authors declare no conflict of interest.

Acknowledgements

Supporting Information Available.

REFERENCES

1. Bowler C, Vardi A, Allen AE (2010) Oceanographic and biogeochemical insights from diatom genomes. Annu Rev Marine Sci 2:333–365

2. Nelson DM, Tréguer P, Brzezinski MA, Leynaert A, Quéguiner B (1995) Production and dissolution of biogenic silica in the ocean: Revised global estimates, comparison with regional data and relationship to biogenic sedimentation. Global Biogeochem Cycles 9:359–372

3. Bowler C, Allen AE, Badger JH et al (2008) The *Phaeodactylum* genome reveals the evolutionary history of diatom genomes. Nature 456:239–244

4. Grouneva I, Gollan PJ, Kangasjärvi S, Suorsa M, Tikkanen M, Aro E-M (2013) Phylogenetic viewpoints on regulation of light harvesting and electron transport in eukaryotic photosynthetic organisms. Planta 237:399–412

5. Nagao R, Moriguchi A, Tomo T, Niikura A, Nakajima S, Suzuki T, Okumura A, Iwai M, Shen R-S, Ikeuchi M, Enami I (2010) Binding and functional properties of five extrinsic proteins in oxygen-evolving photosystem II from a marine centric diatom, *Chaetoceros gracilis*. J Biol Chem 285:29191–29199

6. Nagao R, Ishii A, Tada O, Suzuki T, Dohmae N, Okumura A, Iwai M, Takahashi T, Kashino Y, Enami I (2007) Isolation and characterization of oxygen-evolving thylakoid membranes and Photosystem II particles from a marine diatom *Chaetoceros gracilis*. Biochim Biophys Acta 1767:1353–1362

7. Veith T, Büchel C (2007) The monomeric photosystem I-complex of the diatom *Phaeodactylum tricornutum* binds specific fucoxanthin chlorophyll proteins (FCPs) as light-harvesting complexes. Biochim Biophys Acta 1767:1428–1435

8. Akazaki H, Kawai F, Hosokawa M, Hama T, Chida H, Hirano T, Lim B-K, Sakurai N, Hakamata W, Park S-Y, Nishio T, Oku T (2009) Crystallization and structural analysis of cytochrome c_6 from the diatom *Phaeodactylum tricornutum* at 1.5 Å resolution. Biosci Biotechnol Biochem 73:189–191

9. Peers G, Price NM (2006) Copper-containing plastocyanin used for electron transport by an oceanic diatom. Nature 441:341-344

10. Ben-Shem A, Frolow F, Nelson N (2003) Crystal structure of plant photosystem I. Nature 426:630–635

11. Fromme P, Melkozernov A, Jordan P, Krauss N (2003) Structure and function of photosystem I: interaction with its soluble electron carriers and external antenna systems. FEBS Lett 555:40–44

12. Busch A, Hippler M (2011) The structure and function of eukaryotic photosystem I. Biochim Biophys Acta 1807:864–877

13. Hervás M, Navarro JA, De la Rosa MA (2003) Electron transfer between soluble proteins and membrane complexes in photosynthesis. Acc Chem Res 36:798–805

14. Hervás M, Navarro JA, Díaz A, De la Rosa MA (1996) A comparative thermodynamic analysis by laser-flash absorption spectroscopy of photosystem I reduction by plastocyanin and cytochrome c_6 in *Anabaena* PCC 7119, *Synechocystis* PCC 6803, and spinach. Biochemistry 35:2693–2698

15. Molina-Heredia FP, Hervás M, Navarro JA, De la Rosa MA (2001) A single arginyl residue in plastocyanin and cytochrome c_6 from the cyanobacterium *Anabaena sp.* PCC 7119 is required for efficient reduction of photosystem I. J Biol Chem 276:601–605

16. Hervás M, Díaz-Quintana A, Kerfeld C, Krogmann D, De la Rosa MA, Navarro JA (2005) Cyanobacterial Photosystem I lacks specificity in its interaction with cytochrome c_6 electron donors. Photosynth Res 83:329–333

17. Bernal-Bayard P, Molina-Heredia FP, Hervás M, Navarro JA (2013) Photosystem I reduction in diatoms: as complex as the green lineage systems but less efficient. Biochemistry 52:8687–8695

18. Hervás M, Navarro JA, Díaz A, Bottin H, De la Rosa MA (1995) Laser-flash kinetic analysis of the fast electron transfer from plastocyanin and cytochrome c_6 to photosystem I. Experimental evidence on the evolution of the reaction mechanism. Biochemistry 34:11321–11326

19. Hope AB (2000) Electron transfer amongst cytochrome f, plastocyanin and photosystem I: kinetics and mechanisms. Biochim Biophys Acta 1456:5–26

20. De la Rosa MA, Navarro JA, Díaz-Quintana A, De la Cerda B, Molina-Heredia FP, Balme A, Murdoch PS, Díaz-Moreno I, Durán RV, Hervás M (2002) An evolutionary analysis of the reaction mechanisms of photosystem I reduction by cytochrome c_6 and plastocyanin. Bioelectrochem 55:41–45

21. Navarro JA, Hervás M, De la Rosa MA (2011) Purification of plastocyanin and cytochrome c_6 from plants, green algae, and cyanobacteria. In: Carpentier R (ed) Photosynthesis Research Protocols vol. 684, Humana Press Inc, Totowa, NJ, pp 79–94

22. Molina-Heredia FP, Wastl J, Navarro JA, Bendall D, Hervás M, Howe C, De la Rosa MA (2003) A new function for an old cytochrome? Nature 424:33–34

23. Molina-Heredia FP, Balme A, Hervás M, Navarro JA, De la Rosa MA (2002) A comparative structural and functional analysis of cytochrome c_M, cytochrome c_6 and plastocyanin from the cyanobacterium *Synechocystis* sp. PCC 6803. FEBS Lett 517:50–54

24. Mathis P, Sétif P (1981) Near infra-red absorption spectra of the chlorophyll *a* cations and triplet state *in vitro* and *in vivo*. Isr J Chem 21:316–320

25. Arnon DI (1949) Copper enzymes in isolated chloroplasts. Plant Physiol 24:1–15

26. Hervás M, Navarro JA (2011) Effect of crowding on the electron transfer process from plastocyanin and cytochrome c_6 to photosystem-I: a comparative study from cyanobacteria to green algae. Photosynth Res 107:279–286

27. Sigfridsson K, He S, Modi S, Bendall DS, Gray J, Hansson Ö (1996) A comparative flash-photolysis study of electron transfer from pea and spinach plastocyanins to spinach photosystem I. A reaction involving a rate-limiting conformational change. Photosynth Res 50:11–21

28. Tollin G, Meyer TE, Cusanovich MA (1986) Elucidation of the factors which determine reaction-rate constants and biological specificity for electron-transfer proteins. Biochim Biophys Acta 853:29–41

29. Amunts A, Toporik H, Borovikova A, Nelson N (2010) Structure determination and improved model of plant photosystem I. J Biol Chem 285:3478–3486

30. Jolley C, Ben-Shem A, Nelson N, Fromme P (2005) Structure of plant photosystem I revealed by theoretical modeling. J Biol Chem 280:33627–33636

31. Altschul SF, Gish W, Miller W, Myers EW, Lipman DJ (1990) Basic local alignment search tool. J Mol Biol 215:403–410

32. Eswar N, Webb B, Marti-Renom MA, Madhusudhan MS, Eramian D, Shen MY, Pieper U, Sali A (2007) Comparative protein structure modeling using MODELLER. Curr Protoc Protein Sci, Unit 2.9:1–31

33. Shen MY, Sali A (2006) Statistical potential for assessment and prediction of protein structures. Protein Sci 15:2507–2524

34. Pettersen EF, Goddard TD, Huang CC, Couch GS, Greenblatt DM, Meng EC, Ferrin TE (2004) UCSF Chimera-a visualization system for exploratory research and analysis. J Comput Chem 25:1605–1612

35. Redinbo MR, Cascio D, Choukair MK, Rice D, Merchant S, Yeates TO (1993) The 1.5-Å crystal structure of plastocyanin from the green alga *Chlamydomonas reinhardtii*. Biochemistry 32:10560–10567

36. Gabb HA, Jackson RM, Sternberg MJ (1997) Modelling protein docking using shape complementarity, electrostatics and biochemical information. J Mol Biol 272:106–120

37. Chen R, Weng Z (2003) A novel shape complementarity scoring function for protein-protein docking. Proteins 51:397–408

38. Cheng TM, Blundell TL, Fernandez-Recio J (2007) pyDock: electrostatics and desolvation for effective scoring of rigid-body protein-protein docking. Proteins 68:503–15

39. Jiménez-García B, Pons C, Fernández-Recio J (2013) pyDockWEB: a web server for rigid-body protein-protein docking using electrostatics and desolvation scoring. Bioinformatics 29:1698–1699

40. Jo S, Kim T, Iyer VG, Im W (2008) CHARMM-GUI: a web-based graphical user interface for CHARMM. J Comput Chem 29:1859–1865

41. Abagyan R, Lee WH, Raush E, Budagyan L, Totrov M, Sundstrom M, Marsden BD (2006) Disseminating structural genomics data to the public: from a data dump to an animated story. TRENDS Biochem Sci 31:76–78

42. Sigfridsson K, Young S, Hansson Ö (1997) Electron transfer between spinach plastocyanin mutants and photosystem 1. Eur J Biochem 245:801–812

43. Sommer F, Drepper F, Hippler M (2002) The luminal helix l of PsaB is essential for recognition of plastocyanin or cytochrome c_6 and fast electron transfer to photosystem I in *Chlamydomonas reinhardtii*. J Biol Chem 277:6573–6581

44. Drepper F, Hippler M, Nitschke W, Haehnel W (1996) Binding dynamics and electron transfer between plastocyanin and photosystem I. Biochemistry 35:1282–1295

45. Kohzuma T, Inoue T, Yoshizaki F, Sasakawa Y, Onodera K, Nagatomo S, Kitagawa T, Uzawa S, Isobe Y, Sugimura Y, Gotowda M, Kai Y (1999) The structure and unusual pH dependence of plastocyanin from the fern *Dryopteris crassirhizoma*. The protonation of an active site histidine is hindered by π–π interactions. J Biol Chem 274:11817–11823

46. Navarro JA, Lowe CE, Amons R, Kohzuma T, Canters GW, De la Rosa MA, Ubbink M, Hervás M (2004) Functional characterization of the evolutionarily divergent fern plastocyanin. Eur J Biochem 271:3449–3456

47. Díaz-Quintana A, Hervás M, Navarro JA, De la Rosa MA (2008) Plastocyanin and cytochrome c_6: the soluble electron carriers between the cytochrome b_6f complex and photosystem I. In: Fromme P (ed) Photosynthetic Protein Complexes: A Structural Approach. Wiley-VCH Verlag Gmbh & Co. KGaA, Weinheim. pp 181–200

48. Frazão C, Soares CM, Carrondo MA, Pohl E, Dauter Z, Wilson KS, Hervás M, Navarro JA, De la Rosa MA, Sheldrick GM (1995) Ab initio determination of the crystal structure of cytochrome c_6 and comparison with plastocyanin. Structure 3:1159–1169

49. Mazor Y, Borovikova A, Nelson N (2015) The structure of plant photosystem I super-complex at 2.8 Å resolution. eLife 4:e07433. DOI: 10.7554/eLife.07

50. Sommer F, Drepper F, Haehnel W, Hippler M (2004) The hydrophobic recognition site formed by residues PsaA-Trp651 and PsaB-Trp627 of photosystem I in *Chlamydomonas reinhardtii* confers distinct selectivity for binding of plastocyanin and cytochrome c_6. J Biol Chem 279:20009–20017

51. Sommer F, Drepper F, Haehnel W, Hippler M (2006) Identification of precise electrostatic recognition sites between cytochrome c_6 and the photosystem I subunit PsaF using mass spectrometry. J Biol Chem 281:35097–35103
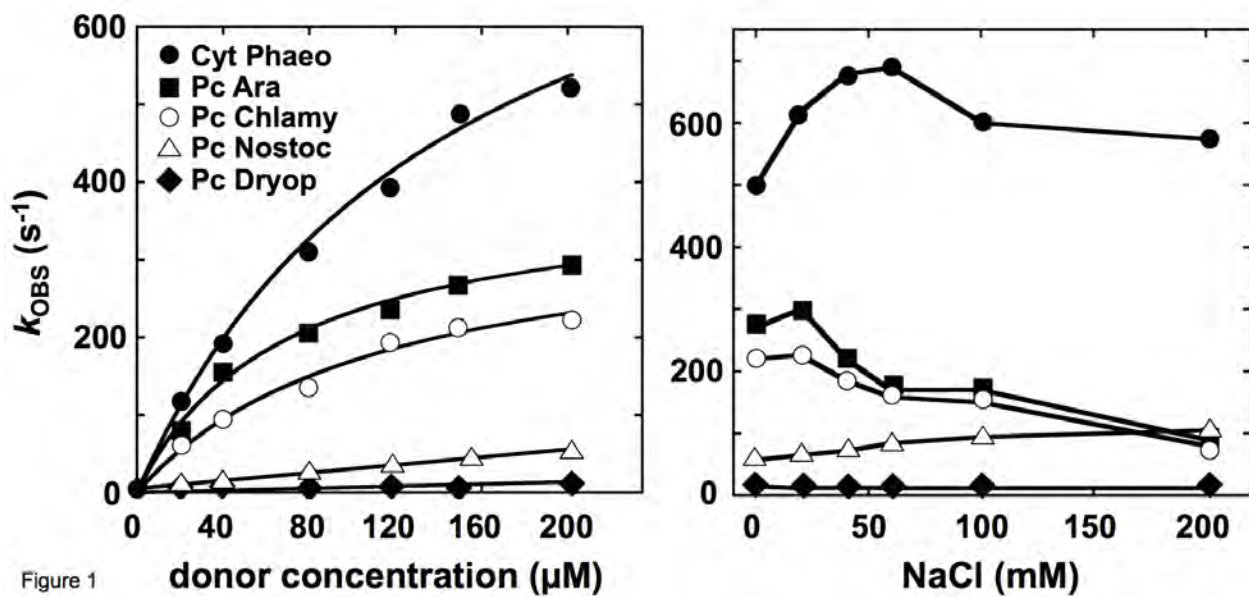
Figure 1

Figure 2

10 ms

10 ms

40 ms

ΔAbs (830 nm) →

A

B

C

A: WT Pc, no salt
B: WT Pc + 0.2 M NaCl
C: E85K Pc + 0.2 M NaCl

Phaeodactylum Cyt

Chlamydomonas Pc

Q88
V93
E85

E85V   E85K   Q88R   V93K

Figure 3

- ● Pc WT
- ○ E85K
- □ Q88R
- △ E85K/Q88R
- ◇ V93K
- ■ E85V

k_{OBS} (s^{-1})
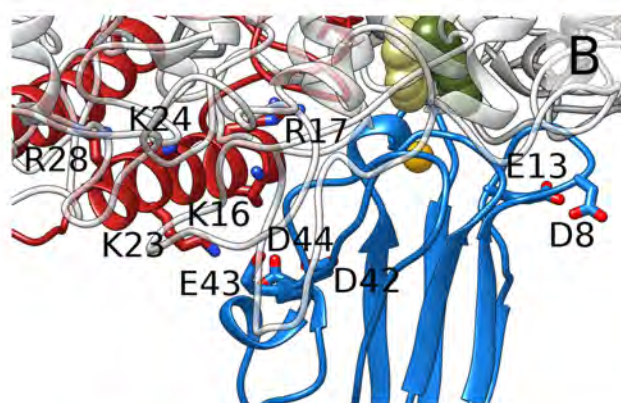
donor concentration (μM)

NaCl (mM)
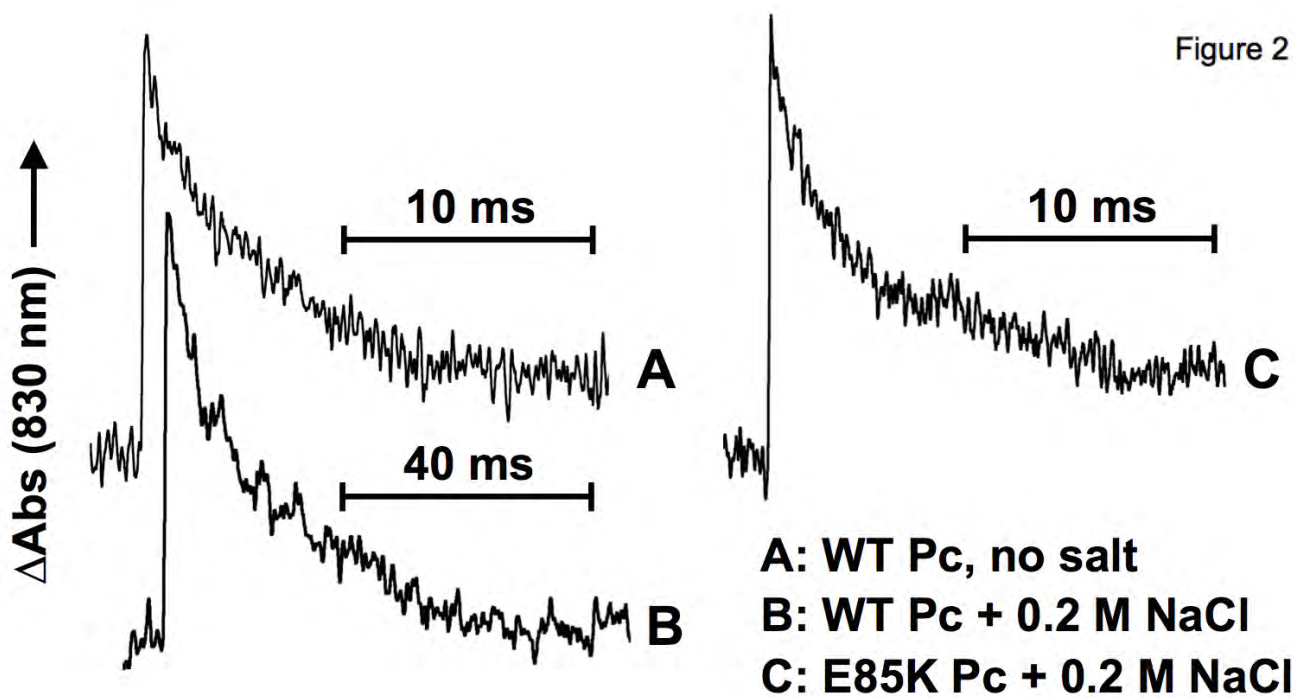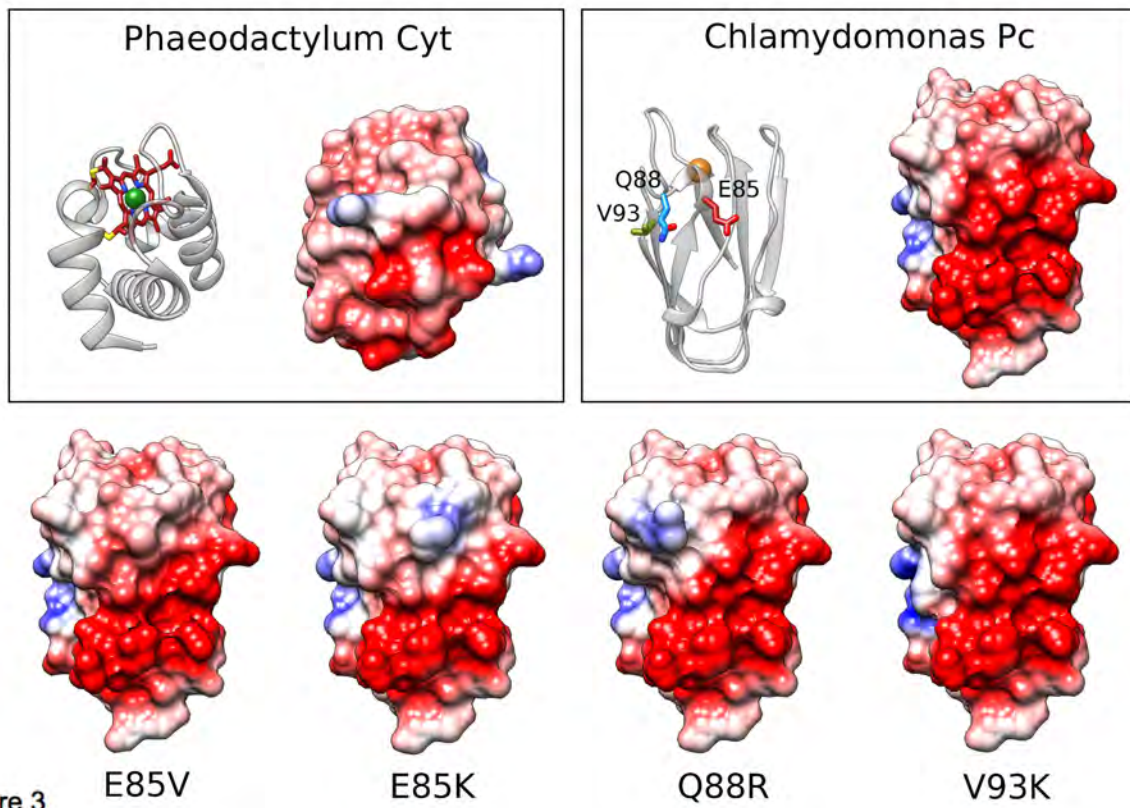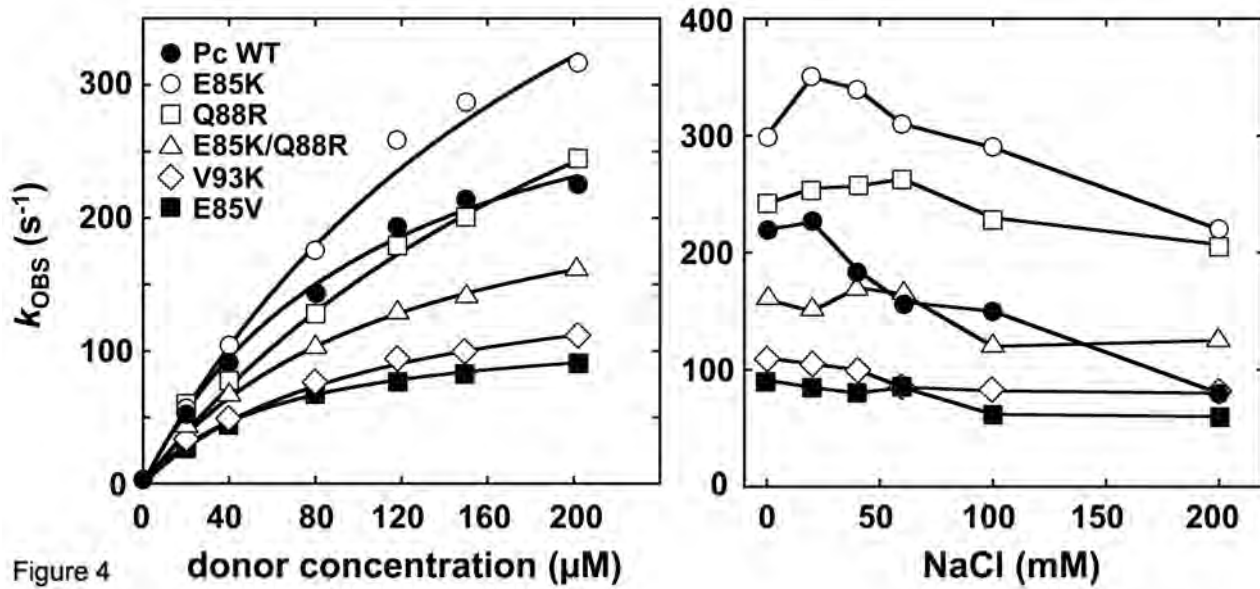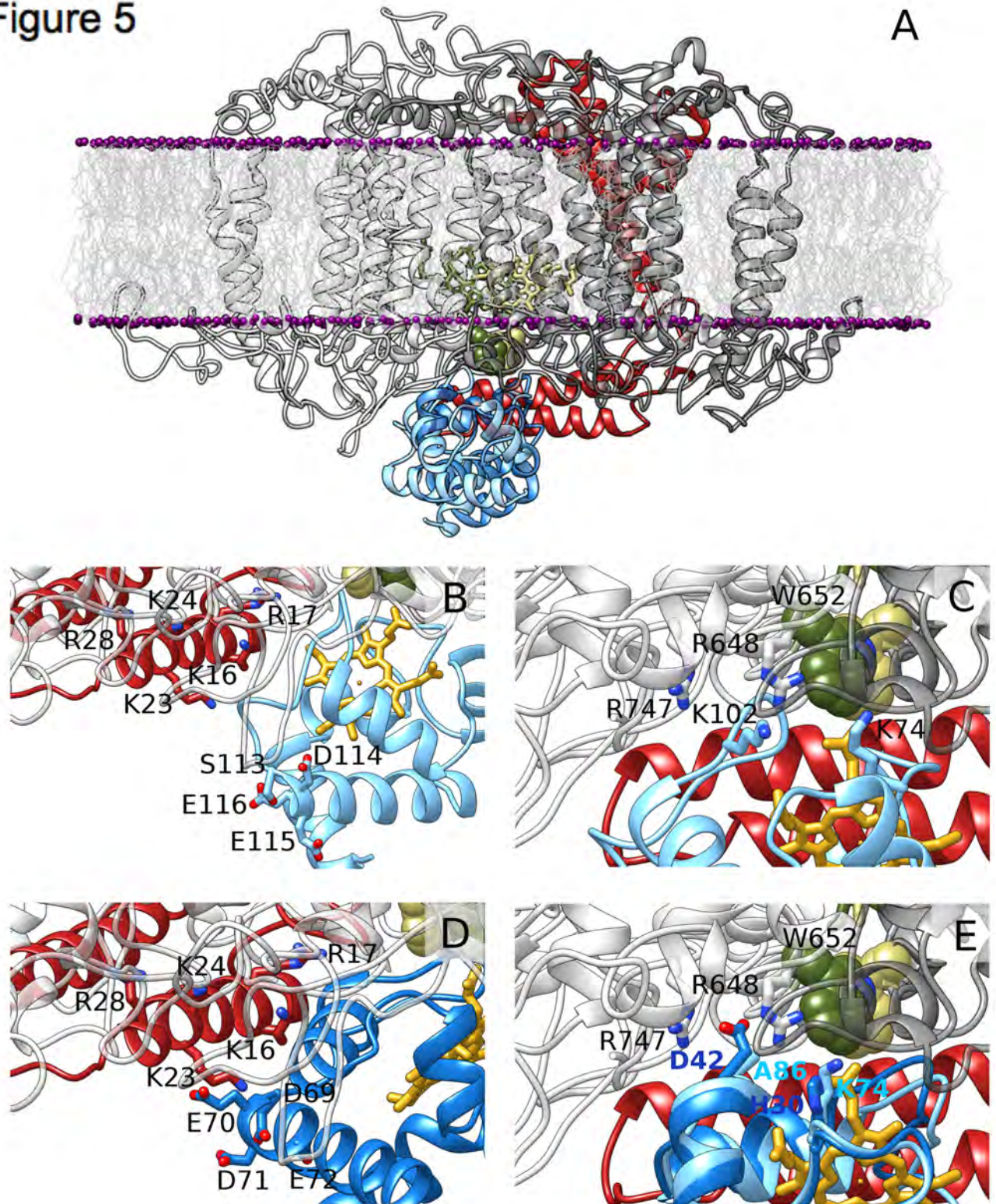
Figure 4

Figure 5

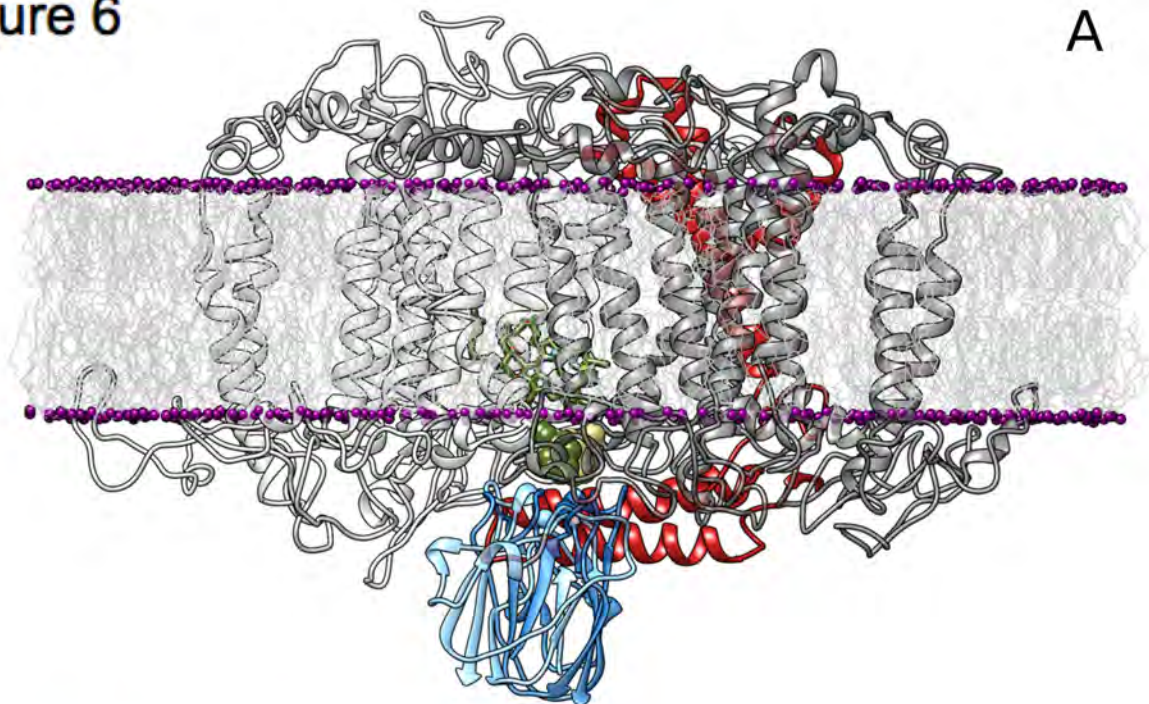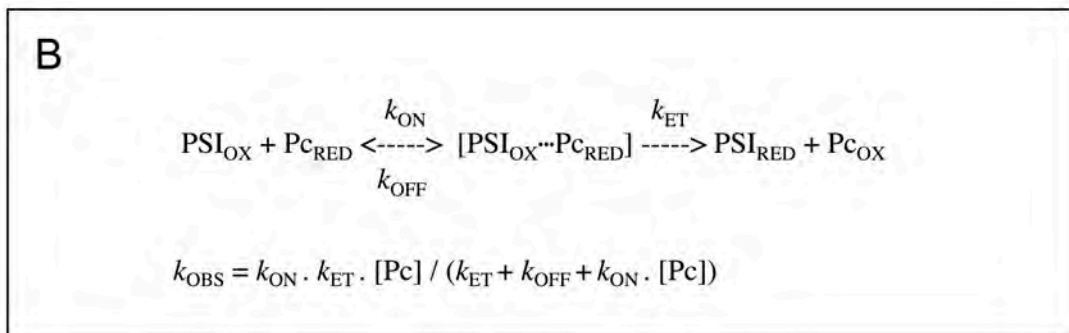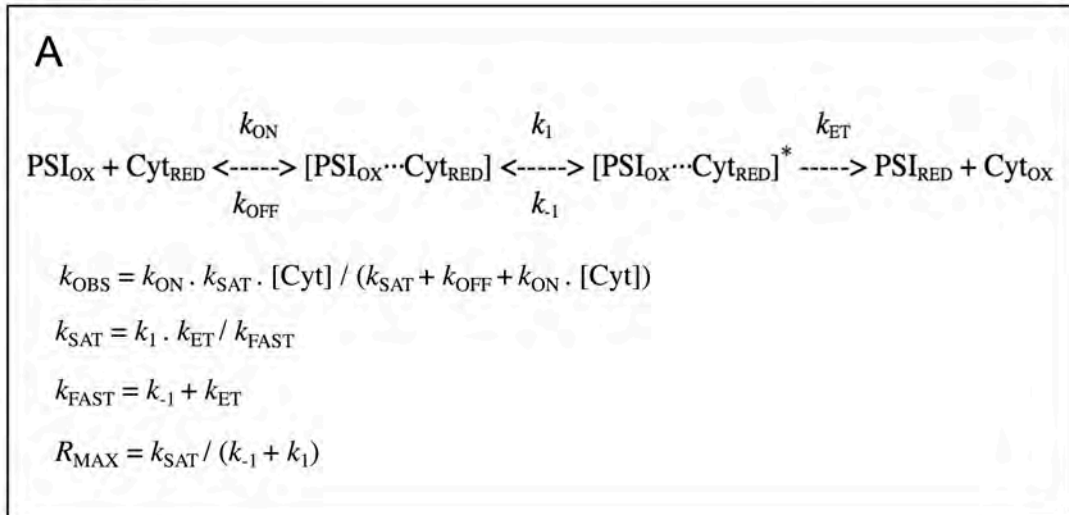Figure 6
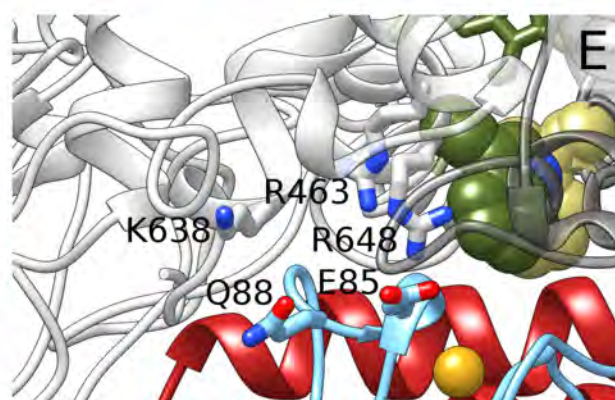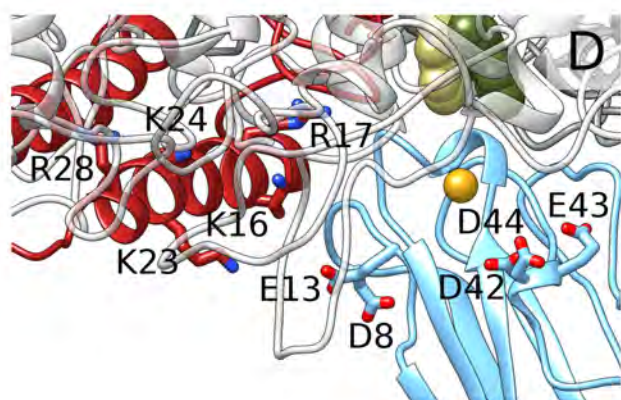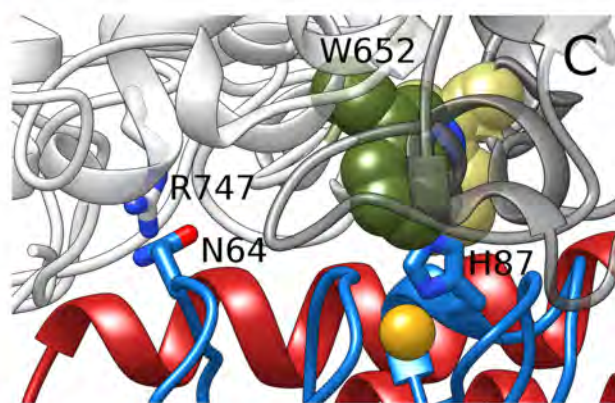
```
ATGAAGAAAATCTTCTCTCTGGTTCTGCTGGGTATCGCGCTGTTCACCTTCGCGTTCTCTTCT
 M   K   K   I   F   S   L   V   L   L   G   I   A   L   F   T   F   A   F   S   S

CCGGCGCTGGCTGACGCGACCGTTAAACTGGGTGCGGACTCTGGTGCTCTGGAATTCGTTCCG
 P   A   L   A   D   A   T   V   K   L   G   A   D   S   G   A   L   E   F   V   P

AAAACCCTGACCATCAAATCTGGTGAGACCGTAAACTTCGTTAATAACGCGGGTTTCCCGCAC
 K   T   L   T   I   K   S   G   E   T   V   N   F   V   N   N   A   G   F   P   H

AACATCGTTTTCGACGAAGACGCGATCCCGTCTGGTGTTAACGCAGACGCTATCTCTCGTGAC
 N   I   V   F   D   E   D   A   I   P   S   G   V   N   A   D   A   I   S   R   D

GACTACCTGAACGCGCCTGGTGAAACCTACTCTGTAAAACTCACCGCGGCAGGTGAATACGGT
 D   Y   L   N   A   P   G   E   T   Y   S   V   K   L   T   A   A   G   E   Y   G

TACTACTGCGAACCGCACCAGGGTGCAGGTATGGTTGGTAAAATCATCGTTCAGTAATGA
 Y   Y   C   E   P   H   Q   G   A   G   M   V   G   K   I   I   V   Q  StopStop
```

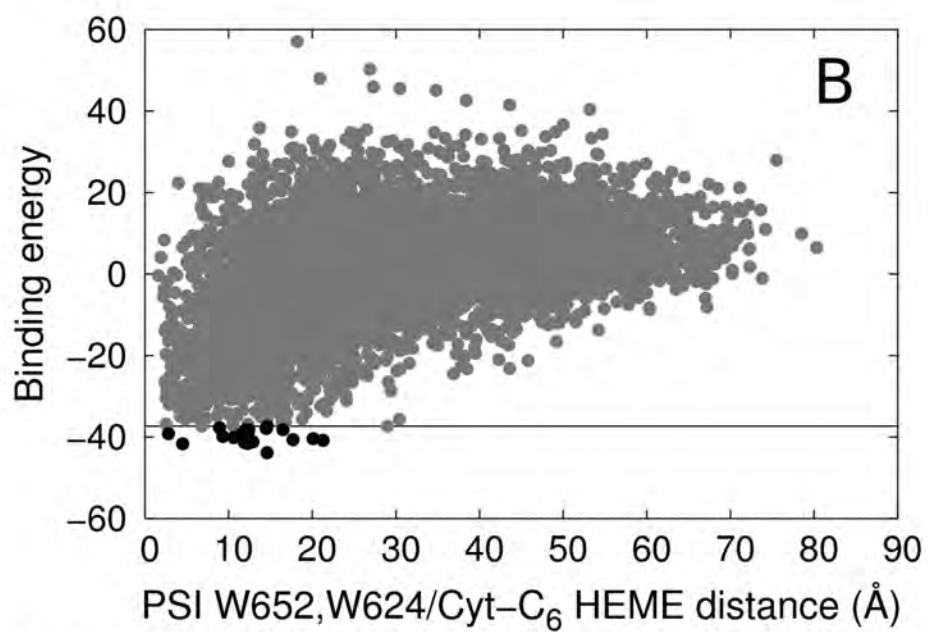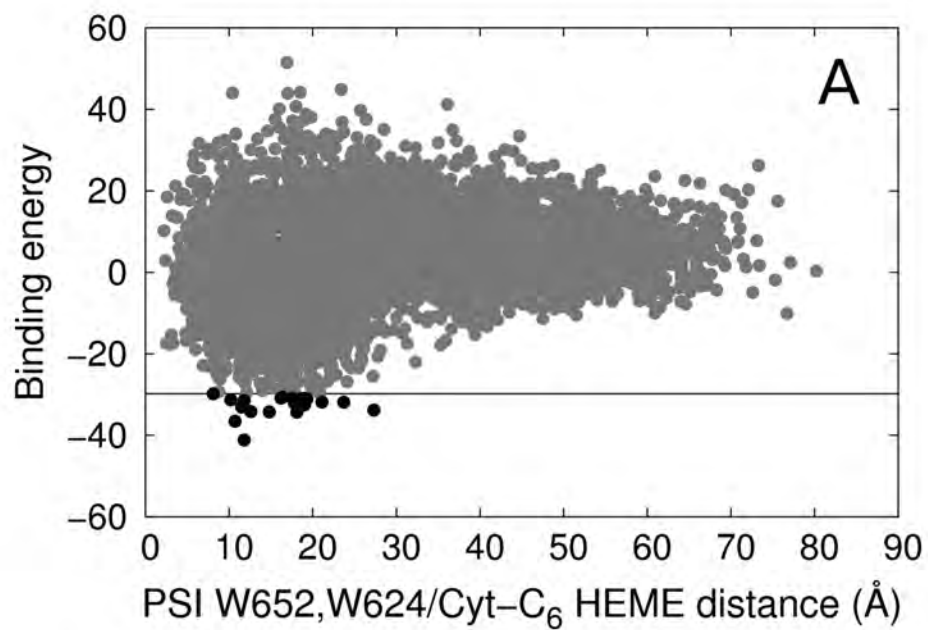| Name	Sequence (5' ⟶ 3')
E85K_D	GGTTACTACTGCAAACCGCACCAGGG
E85K_R	CCCTGGTGCGGTTTGCAGTAGTAACC
E85V_D	GGTTACTACTGCGTTCCGCACCAGGG
E85V_R	CCCTGGTGCGGAACGCAGTAGTAACC
Q88R_D	GAACCGCACCGTGGTGCAGGTATGG
Q88R_R	CCATACCTGCACCACGGTGCGGTTC
V93K_D	CAGGTATGAAAGGTAAAATCATC
V93K_R	GATGATTTTACCTTTCATACCTG
E85K_Q88R_D	GCAAACCGCACCGTGGTGCAGGTATGG
E85K_Q88R_R	CCATACCTGCACCACGGTGCGGTTTGC

Figure S1

A

$$PSI_{OX} + Cyt_{RED} \overset{k_{ON}}{\underset{k_{OFF}}{\longleftrightarrow}} [PSI_{OX} \cdots Cyt_{RED}] \overset{k_1}{\underset{k_{-1}}{\longleftrightarrow}} [PSI_{OX} \cdots Cyt_{RED}]^* \overset{k_{ET}}{\longrightarrow} PSI_{RED} + Cyt_{OX}$$

$$k_{OBS} = k_{ON} \cdot k_{SAT} \cdot [Cyt] \, / \, (k_{SAT} + k_{OFF} + k_{ON} \cdot [Cyt])$$

$$k_{SAT} = k_1 \cdot k_{ET} \, / \, k_{FAST}$$

$$k_{FAST} = k_{-1} + k_{ET}$$

$$R_{MAX} = k_{SAT} \, / \, (k_{-1} + k_1)$$

B

$$PSI_{OX} + Pc_{RED} \overset{k_{ON}}{\underset{k_{OFF}}{\longleftrightarrow}} [PSI_{OX} \cdots Pc_{RED}] \overset{k_{ET}}{\longrightarrow} PSI_{RED} + Pc_{OX}$$

$$k_{OBS} = k_{ON} \cdot k_{ET} \cdot [Pc] \, / \, (k_{ET} + k_{OFF} + k_{ON} \cdot [Pc])$$

Figure S3

Figure S4